IMPACT BASIN RELAXATION ON RHEA AND IAPETUS AND RELATION TO PAST HEAT FLOW

Oliver L. White[a], Paul M. Schenk[a], and Andrew J. Dombard[b]

[a]Lunar and Planetary Institute, 3600 Bay Area Blvd., Houston, TX 77058
[b]Dept. of Earth and Environmental Sciences, University of Illinois at Chicago, 845 W. Taylor St., Chicago, IL 60607

Manuscript pages: 35
Figures: 6
Tables: 5

Present address of corresponding author: Oliver White
Lunar and Planetary Institute
3600 Bay Area Boulevard
Houston
Texas
77058
white@lpi.usra.edu
281-309-8152 (Cell)
281-486-2148 (Work)

Paul Schenk: schenk@lpi.usra.edu
Andrew Dombard: adombard@uic.edu

Abstract. Evidence for relaxation of impact crater topography has been observed on many icy satellites, including those of Saturn, and the magnitude of relaxation can be related to past heat flow (e.g. Moore et al., 2004; Dombard and McKinnon, 2006). We use new global digital elevation models of the surfaces of Rhea and Iapetus generated from Cassini data to obtain crater depth/diameter data for both satellites and topographic profiles of large basins on each. In addition to the factor of 3 lower amplitude of global topography on Rhea compared to Iapetus, we show that basins on Iapetus >100 km in diameter show little relaxation compared to similar sized basins on Rhea. Because of the similar gravities of Rhea and Iapetus, we show that Iapetus basin morphologies can be used to represent the initial, unrelaxed morphologies of the Rhea basins, and we use topographic profiles taken across selected basins to model heat flow on both satellites. We find that Iapetus has only experienced radiogenic heat flow since formation, whereas Rhea must have experienced heat flow reaching a few tens of mW m^{-2}, although this heat flow need only be sustained for as little as several million years in order to achieve the observed relaxation magnitudes. Rhea experienced a different thermal history from Iapetus, which we consider to be primarily related to their different formation mechanisms and locations within the Saturnian system. A recent model for the formation of Saturn's mid-sized icy satellites interior to and including Rhea (Charnoz et al., 2011) describes how Rhea's orbit would have expanded outwards after its accretion from a giant primordial ring, which would have instigated early heating through rapid despinning and tidal interaction with Saturn and other satellites. Rhea's basins would therefore be required to have formed within the first few tens of Myr of Rhea's formation in order to relax due of this heating, and if so may provide an important anchor point for Saturn system chronology. None of these heating mechanisms are viable for Iapetus in its isolated position far from Saturn, and as such it has remained dynamically inert since formation, confirming conclusions based on thermal modeling of Iapetus' interior. Rapid and complete relaxation and subsequent erosion by bombardment of a 'first generation' of large basins on Rhea is regarded as an explanation for the lower counts of large basins on Rhea relative to Iapetus, and the overall lower amplitude of topography on Rhea compared to Iapetus.

1. Introduction

The mid-sized icy satellites of Saturn offer an excellent natural laboratory for understanding the geological diversity of different-sized icy satellites and their interactions within a complex planetary system (Jaumann et al., 2009). Our knowledge of the geological and thermal histories of these satellites was first shaped by the Voyager spacecraft, which provided an initial, cursory view of these objects during their flybys in 1980 and 1981 (Smith et al., 1981, 1982; Gehrels and Matthews, 1984; Morrison et al., 1986; Moore et al., 2004; Orton et al., 2009). The Cassini spacecraft, since its orbit insertion around Saturn in 2004 (Dougherty et al., 2009; Seal and Buffington, 2009) has greatly expanded our understanding of the surface geology and interiors of the satellites. A notable early discovery from Voyager imagery was that the floors of some craters on Enceladus, Dione and possibly Rhea had become uplifted since formation, a phenomenon attributed to viscous relaxation of the icy crusts of these bodies (Passey, 1983; Schenk, 1989; Moore et al., 2004). The magnitude of crater relaxation differs between satellites. Schenk (1989) first estimated the relaxation states of large impact basins on the Saturnian satellites through extrapolation of the depth/diameter (d/D) fits at smaller crater diameters. The scale of viscous relaxation of a crater is a function of the ductile rheological properties of the satellite (which are themselves sensitive to heat flow), as well as the timescale over which the crater has been relaxing. Examination of relaxed crater populations can therefore in principle be exploited to probe the thermal histories of these icy satellites (e.g., Dombard and McKinnon, 2006).

The survey of crater morphologies on the Saturnian icy satellites performed by Schenk (1989), which was based on Voyager imagery, achieved d/D measurements for 226 craters on Mimas, Tethys, Dione, and Rhea down to a crater diameter of ~5 km. These measurements were obtained using photoclinometry (PC) (e.g., Bonner and Schmall, 1973; Schenk and Williams, 2004) and shadow lengths, as useful Voyager stereo coverage was limited mostly to Rhea (Schenk, 1989). Voyager-based depth measurements were valid for the large craters that were observed, but as with Galileo-based updated measurements of crater depths on Ganymede and Callisto (Schenk, 2002), measurements derived from Cassini data have shown that Voyager-based measurements of small craters on the Saturnian satellites are too shallow due to marginally resolved central features. In the decade since Cassini arrived at Saturn, PC of low-Sun regions and stereo image analysis have been applied to Cassini imagery to create nearly global stereo digital elevation models (DEMs) of the Saturnian mid-sized icy satellites (e.g. Moore and Schenk, 2007; White and Schenk, 2011; Bland et al., 2012; Phillips et al., 2012), supplemented by regional stereo- and PC-derived DEMs.

In this work, we have used stereo- and PC-derived DEMs to measure the dimensions of more than 180 craters on Rhea and Iapetus, the large impact basins of which display quite different relaxation states: those on Rhea are relaxed, whereas those on Iapetus are unrelaxed. Rhea and Iapetus display surface gravities that are similar enough (0.265 m s^{-2} and 0.224 m s^{-2} respectively) such that the effect of inverse scaling of surface gravity with d/D ratio for complex craters (Quaide et al., 1965; Hartmann, 1972; Melosh, 1977; Pike, 1980) is negligible when comparing the morphologies of impact basins on the two satellites. In addition, while higher impactor velocities may be expected on Rhea due to its closer proximity to Saturn, and which may influence initial d/D ratios relative to Iapetus, preliminary measurements of crater dimensions on these satellites have not revealed any dichotomy in the d/D ratios of unrelaxed complex craters that may originate from differences in impactor velocity (White and Schenk, 2011). We compare the d/D plots of craters on both satellites to identify the onset diameter of crater relaxation on Rhea, and the magnitude of relaxation of large basins on that satellite. We also model timescales and heat flows associated with relaxation using idealized topographic profiles plotted across similar-sized basins on both satellites in order to place constraints on the thermal histories of Rhea and Iapetus.

2. Derivation of DEMs and Crater Measurement

Stereo analysis of Cassini images uses an ISIS-based automated scene recognition algorithm that attempts to match albedo patterns in finite-sized patches in each of two stereo images (Schenk et al., 2004), and has been successfully applied to the Galilean satellites (Schenk et al., 1997; Schenk and Bulmer, 1998). Approximately 80% of the surface of Rhea and 50% to 60% of Iapetus are mappable in stereo at better than 100 m vertical resolution and better than 1 km horizontal resolution. Stereo DEMs are reliable at long wavelength, regional scales, but are unable to resolve fine scale topographic features that are smaller than approximately five times the resolution of the poorest resolution image in the stereo pair due to pixel averaging. PC derives topography through estimation of slope based on surface brightness, and greatly extends topographic sensitivity beyond that available through stereo imaging. We employ a PC algorithm developed for rapid 2-dimensional PC mapping that includes modeling of local albedo changes (e.g. Schenk and Williams, 2004). PC DEMs achieve resolutions at the pixel scale and so are more suited to mapping local-scale topography, but are subject to significant topographic uncertainty over longer distances. PC DEMs are therefore merged with the stereo DEMs (where available) in order to control the long wavelength component and to produce full-pixel scale topography over most of the surface. More detailed descriptions of the mapping methods employed are contained in Schenk (1989) and Schenk et al. (2004). Figure 1 presents the global stereo DEMs we have derived for Rhea and Iapetus. The DEMs are stretched to the same degree (-8 km to +8 km), highlighting the contrast in vertical relief of the topography on Iapetus and Rhea, which differs by a factor of ~3 (Castillo-Rogez et al., 2007; Giese et al., 2008).

Crater diameter and depth measurements using the lower resolution, stereo-derived global DEMs of Rhea and Iapetus are confined to craters that are tens of kilometers in diameter. Measurements from merged PC/stereo or high resolution stereo DEMs may include craters down to a few kilometers in diameter. For each of the DEMs used, Table 1 presents the coverage, resolutions, and the number of craters for which measurements were made. For each profile, the depth is the mean value of the two depths measured from the nadir to the two rim crests, and the diameter is measured from rim crest to rim crest. Different numbers of profiles are taken across craters according to their size and complexity. For the largest impact basins that are hundreds of kilometers across, at least six profiles are necessary in order to obtain mean depth and diameter values that are properly representative of the whole basin; for simple craters that are several kilometers across, three or four profiles will suffice. In general the freshest appearing craters, i.e. those that appear to show sharp rims, are measured in order to establish the reference baseline for unmodified crater shapes; the exception to this is the large impact basins, which due to their relative infrequency are measured regardless of their preservation state.

3. Crater Morphologies on Rhea and Iapetus

d/D ratios have been measured for 189 craters (105 on Rhea and 85 on Iapetus) that range in diameter from 1.5 km to 565 km. We divide crater morphologies into three classes (Pike, 1974, 1980; Williams and Zuber, 1998): bowl- or cone-shaped simple craters, complex craters with flat floors and (sometimes) central peaks, and impact basins, which are essentially an extension of complex crater morphology, but which display a central plateau, ring complex, and/or a central pit. Fig. 2 shows d/D plots for Rhea and Iapetus, and Table 2 presents least squares statistics for the d/D plots. Iapetus displays more craters above 100 km in diameter (20) than Rhea (13), yet due to the poorer stereo coverage achieved by Cassini at Iapetus compared to Rhea, the number of craters >100 km in diameter that we have obtained measurements for is similar on Iapetus (4) and Rhea (5).

The simple-complex d/D transition diameter is similar for Rhea (4.71 km) and Iapetus (4.52 km), a consequence of the similar gravities of the two satellites. The complex crater d/D best-fit trend slopes for Rhea and Iapetus (0.478 and 0.567 respectively) are also similar, although the simple trend slope for Rhea is slightly shallower (0.808) than the lunar (1.013) and Iapetus (1.047) trends. The 95% confidence limits for the Rhea and Iapetus slopes do not overlap. This is likely a consequence of the varying processing techniques and resolutions of the Rhea DEMs that were used to measure simple craters (two merged stereo/PC DEMs with lateral resolutions of 0.14 and 0.19 km/px) relative to the Iapetus DEMs (one stereo DEM of lateral resolution 0.1 km/px).

The most pronounced divergence between the Rhea and Iapetus trends occurs at a crater diameter of ~100 km. A single best-fit line of slope 0.552 fits both the Iapetus complex craters and large basins when combined, essentially unchanged from the complex-only fit, indicating that Iapetus basins likely retain their initial morphologies and depths. However, at ~100 km the Rhea complex trend of slope 0.478 transitions to a shallower slope of 0.039. The maximum depth attained by Rhea craters is ~6 km. The mean depth of Rhea's impact basins (4.7 km) is 7.2 km shallower than that of Iapetus's basins (11.9 km). The fact that the simple and complex trends for Rhea and Iapetus overlap fairly well, but diverge dramatically above ~100 km indicates that relaxation is evidently minimal for craters of all sizes on Iapetus, but that all large craters on Rhea are relaxed to roughly similar magnitudes. A similar phenomenon can be seen on Ganymede and Callisto (Schenk, 2002), where it has been proposed that there are no unrelaxed large craters (cf. Dombard et al., 2009). We can regard as negligible the effect of surface gravity on the initial d/D ratio of impact basins on both satellites due to their similar gravities, meaning that we assume basins on both satellites initially displayed d/D ratios similar to those shown by the present-day Iapetus basins. We therefore consider unrelaxed basins on Iapetus to represent analogues of the Rhea basins in their initial, unrelaxed state, and so may be used to assess the extent of relaxation experienced by the Rhea basins since formation. We do not consider Herschel basin on Mimas (Thomas and Squyres, 1988) to be an appropriate unrelaxed reference for the Rhea basins (Phillips et al., 2012). Using Herschel would require the extra step of scaling our Rhea measurements based on the d/D trend of Mimas, which has not been sufficiently characterized, and which will not be the same as that of Rhea or Iapetus due to Mimas' smaller gravity (0.064 m s^{-2}) compared to those satellites.

Table 3 lists relaxation fractions for each of the four largest named basins on Rhea relative to the Iapetus best-fit complex crater and basin trend. The apparent depth relaxation fraction (*RF*) is defined as $1 - d_a(t)/d_a(0)$ (Dombard and McKinnon, 2006), where $d_a(0)$ is the depth of the initial, unrelaxed basin and $d_a(t)$ is the depth of the relaxed basin after time, t, has elapsed. In all cases, depth is measured from the initial ground plane to the floor of the basin. The standard measure in crater relaxation studies is the time needed for the initial crater depth to decrease by a factor of $1/e$ (e.g., Passey, 1982). The relaxation fraction for this factor is equal to $1 - 1/e \approx 0.632$. *RF* values for Powehiwehi, Tirawa, and Mamaldi are close to or exceed this value, yet that for Izanagi is considerably less.

In order to simulate the long-term relaxation of impact basin topography on Rhea, we will use averaged profiles taken across four impact basins on Rhea and Iapetus at 2 different representative sizes. The multiple profiles taken across each basin are combined in order to produce a single averaged, symmetrical, 'idealized' profile. The basin profiles are paired based on similarities in diameter: Powehiwehi (268 km diameter) and Naimon (261 km diameter, and which has actually been classified as a complex crater) on Rhea and Iapetus respectively, and Tirawa (397 km diameter) and Falsaron (422 km diameter) on Rhea and Iapetus respectively. Morphology statistics for each basin are collated in Table 4. For each basin pair, the profile of the smaller basin is then scaled such that it matches the diameter of the larger basin (i.e. Tirawa is scaled to fit Falsaron, and Naimon is scaled to fit Powehiwehi), in order that relaxed (Rhea basins) and unrelaxed (Iapetus basins) profiles for the two size classes can be compared. The profiles for each pair are overlain in Fig. 3. The four basins themselves are displayed in visible imagery in Fig. 4.

4. Simulation of Crater Relaxation

The goal of the relaxation simulations is to constrain the thermal evolution of Rhea, i.e., track heat flow through time. Topographic relaxation simulation is achieved using the MSC.Marc finite element package. This package is well suited for study of creeping flow of geological materials, and has been used extensively for the study of crater relaxation in general (Dombard, 2000; Dombard and McKinnon, 2000; Dombard and Gillis, 2001; Dombard and McKinnon, 2006; Dombard et al., 2007, 2009).

Relaxation simulations in these earlier studies have been extensively benchmarked against analytic solutions as well as TEKTON (Dombard and McKinnon, 2006, section 3.2, Fig. 14). We input initial topographic conditions (as represented by the unrelaxed Iapetus basins) in an attempt to evolve the presumed initial basin topography on Rhea, with presumed rheology, into the observed, relaxed Rhea topography. A range of thermal profiles is entered to find which combination of input parameters result in a time-progression most consistent with observation. It should be noted that we are only attempting to match the levels of the observed and simulated basin floors (i.e., the long wavelength component of the basins), and not the summits of the shorter wavelength rims and central peaks. In particular for central peaks, the final elevation can be strongly sensitive to the presence of remnant impact heat (Dombard et al., 2007). For high background heat flow, the presence of impact heat leads to enhanced uplift of the crater center and a high central peak, grading into collapse of the central peak for still higher background heat fluxes. In contrast, the presence of remnant impact heat has little effect on the depth of the basin floor (Dombard et al., 2009).

The procedure applies a finite element mesh to each of the unrelaxed Iapetus basin profiles. We take advantage of the natural axisymmetry of impact craters by simulating one radial plane. The far (side and bottom) boundaries are placed far enough away to have negligible effect on the solution, and the mesh itself is biased to concentrate elements near the basin (usually ~1500-2000 elements total). Material (i.e., density), thermal (i.e., conductivity), and rheological properties are set. Thermal conductivity is determined based on ice temperature in accordance with Klinger (1980): $k_T = 567/T$ W m^{-1}. Rheological properties include elastic (e.g., Gammon et al., 1983) and viscous (Goldsby and Kohlstedt, 2001). A plastic component to the rheology (a continuum approximation for discrete brittle faulting) is not included as plastic failure is generally not a large contributor to deformation associated with relaxation; adding plasticity to a simulation will only affect strongly relaxed craters and cause a reduction in characteristic relaxation time of a factor of ~2, as compared to the many orders of magnitude change in relaxation time from a modest (factor of ~3) change in heat flow (Fig. 10 in Dombard and McKinnon, 2006). A thermal simulation is performed first to find the steady-state temperature structure of the subsurface. Boundary conditions are set to restrict heat flow through the side boundaries, constrain the surface temperature, and impose a regional heat flow. Results from this thermal solution are then applied to the mechanical solution. Motions on the side and bottom boundaries are restricted to free-slip, and a uniform gravity load specific to Rhea is applied. The initial stresses are adjusted to be lithostatic, perturbed by stresses arising from the topography. The simulations are then iterated forward in time, always maintaining force equilibrium, using a time stepping scheme that automatically maximizes the time increment within prescribed tolerances. Errors in our numerical approach are less than a few percent (Dombard, 2000; Dombard and McKinnon, 2006). The resultant topographic profiles are compared with measured profiles of the relaxed Rhea basins.

Crater relaxation is solved in a planar, rather than spherical, geometry. The spherical harmonic degree for the transition from a membrane- to flexure-dominated regime (and hence whether sphericity is important or not) is defined as the square root of satellite radius/lithospheric thickness (Turcotte et al., 1981). Our simulated lithospheres are tens of kilometers thick, meaning the transition is at degrees less than ~8. Our largest craters (~400 km across) deform on a scale of about degree 12, or a shorter wavelength, so membrane stresses (sphericity) are not influential.

How well the goal of constraining Rhea's thermal evolution can be accomplished is dependent on how well input parameters can be constrained. Rates of relaxation are dependent on surface temperature, yet there is some uncertainty in these temperatures because of, for instance, the existence and thermal conductivity of an impact generated regolith (e.g., Passey and Shoemaker, 1982). Furthermore, there is a trade-off between rate of relaxation and the length of time over which a crater relaxes, as surface temperature will change according to the luminosity history of the Sun (Dombard and McKinnon, 2006). In addition, the creep mechanisms that are expected to dominate the flow of water ice, especially in a modest gravity satellite such as Rhea, are sensitive to the size of the ice grains. Grain sizes within icy satellites are unknown, but reasonable estimates of ~0.1 and 1 mm have been made (Barr and McKinnon, 2006; Dombard and McKinnon, 2006), and will be used in our simulations. Smaller grain sizes will result in more efficient relaxation. We also assume that Rhea's rheology is dominated by water ice I. While other components may exist, such as ammonia-water ice and methane clathrate (e.g. McKinnon, 1999; Cruikshank et al., 2005; Waite et al., 2006), water ice I is certainly the cosmochemically dominant ice.

An upper limit on the timescale of relaxation can be determined by estimating the age of the relevant basin using crater counts. We have obtained our own crater counts for Powehiwehi and Tirawa using a global mosaic of Cassini visible images at a resolution of 0.4 km/px. Craters 6 km in diameter and larger are considered in the crater count, and the ages are computed using cratering rate scenarios as described in the case A scenario of Zahnle et al. (2003) and Neukum et al. (2006). The resulting ages are shown in Table 5. Calculated ages using both functions exceed 4 Gyr. The Zahnle function calculates identical ages and age ranges for the two basins; the Neukum function calculates a slightly younger age for Powehiwehi than Tirawa, with ages for both being about 0.34 Gyr younger than those calculated by the Zahnle function.

Present radiogenic heat flow on Rhea and Iapetus is estimated to be 0.72-0.85 mW m^{-2} and 0.36-0.42 mW m^{-2} respectively (Schubert et al., 1986). Assuming that the decrease in mean heat production rate caused by the decay of radioisotopes on Rhea and Iapetus scales with that on Earth, then for these satellites, the heat flow at the time of their formation (~4.5 Ga) should have been a factor of 4.5 greater than present-day values (Turcotte and Schubert, 2002, section 4.5), i.e., ~4 mW m^{-2} on Rhea and ~2 mW m^{-2} on Iapetus. We therefore consider these to be representative values for the primordial radiogenic heat flows of these satellites, and use values of 2 and 4 mW m^{-2} in our simulations. For our simulations that use only radiogenic heat, conditions are selected to maximize the amount of relaxation (i.e. the ancient higher heat flux is maintained over the length of the simulations, and the smallest reasonable grain size of 0.1 mm is used) in order to test whether only radiogenic heating is sufficient to explain the observations.

5. Simulation Results

Figure 5 presents simulated profiles created for each of the two basin size classes with different combinations of heat flow, relaxation timescale, and ice grain size. Figure 6 plots *RF* value against relaxation timescale for each of the combinations. The results show patterns consistent with simulations of relaxed basins on the Galilean satellites (Dombard and McKinnon, 2006). All other parameters being equal, relaxation fractions for Tirawa/Falsaron, the larger basin, are greater than those for Powehiwehi/Naimon due to relaxation being more efficient for longer wavelength topography. For all heat flow scenarios, the relaxation process is mostly complete by several million years after basin formation, with relatively little relaxation occurring thereafter.

The relatively small, radiogenic heat flows yield minimal total relaxation that is insufficient to account for the relaxation observed on Rhea, but which does account for the lack of relaxation observed on Iapetus. For the lowest radiogenic heat flow tested (2 mW m^{-2}), the morphologies of both basins change little even after 4 Gyr and with a grain size of 0.1 mm, yielding an *RF* value of 0.11 for Powehiwehi/Naimon and 0.23 for Tirawa/Falsaron. True relaxation will plausibly be even less than these values considering that the decay of the primordial heat flow was not accounted for in the simulations. These results are comparable with those of Robuchon et al. (2011), who modeled an Iapetus heat flux decreasing from 6 mW m^{-2} at 50 Myr after accretion decreasing to 1.6 mW m^{-2} at 1 Gyr, and concluded that all basins 600 km in diameter or smaller are relaxed by 25% or less.

Combinations of parameters were tested using higher heat flows until profiles were yielded with *RF* values that closely match the present measured values for Powehiwehi and Tirawa (0.66 and 0.58, values which are themselves very close to the *RF* value, 0.632, for the classic relaxation time). A matching profile for Powehiwehi required 30 mW m^{-2} heat flow, and a matching profile for Tirawa required 20 mW m^{-2} heat flow, with ice grain sizes being a nominal 1 mm for both cases (cf. Dombard and McKinnon, 2006). Tested relaxation timescales did not exceed 1 Gyr as the duration of such high heat flows would be limited. Because of the relatively low surface temperature, relaxation timescale has very little influence at these high heat flows; relaxation fractions are virtually identical for relaxation timescales ranging from 10 Myr to 1 Gyr, indicating that even only a very short period of elevated heat flow is necessary to facilitate the required relaxation, consistent with the results of Dombard and McKinnon (2006).

6. Discussion

6.1 Relaxation and heat flow on Iapetus

Our relaxation simulations allow us to make inferences concerning the thermal histories of Rhea and Iapetus. We interpret the large basins on Iapetus to have experienced minimal relaxation since formation based on the linear complex crater and basin d/D trend for Iapetus (Fig. 2). The results of our simulations indicate that in order for such little relaxation to occur, Iapetus must have experienced only radiogenic heat flow, likely not exceeding 2 mW m^{-2}, since the formation of its large impact basins, with no periods of elevated heat flow reaching tens of mW m^{-2}. This interpretation is consistent with current ideas concerning Iapetus' geophysical history and dynamical evolution, and with its location beyond that of the regular Saturian satellite system (Castillo-Rogez et al., 2007). Modeling performed by Castillo-Rogez et al. (2007) indicates that during despinning of Iapetus, an increase in thermal conductivity caused the satellite to develop a thick, mechanically strong lithosphere that preserved Iapetus' 16-hour rotational shape and exaggerated topographic vertical relief. The contribution of tidal heating to Iapetus as a consequence of despinning has been addressed in Castillo-Rogez et al. (2011), who used a model for the dissipation of tidal heat within Iapetus that is based on the experimental literature and accounts for the frequency- and temperature-dependence of ice rheology. Castillo-Rogez et al. (2011) determined that the tidal-stress-generated temperature increase would only be ~15 K integrated over the despinning time (0.9

to 3.7 Gyr, depending on the abundance of impurities within the water ice), and would not contribute considerably to heating of the interior. Iapetus is regarded as having been "dynamically frozen" since formation (McKinnon, 2002; Castillo-Rogez et al., 2007), with orbital characteristics that have remained virtually static (Ward, 1981) and which are defined by a large semi-major axis (equivalent to ~60 Saturn radii) and a low eccentricity (0.0283). The combination of unchanging orbital parameters, a thick lithosphere and a persistent radiogenic heat flow yields a geophysical model for Iapetus that has not been conducive to the relaxation of even its largest impact basins throughout its history, consistent with our basin shape measurements.

6.2 Relaxation and heat flow on Rhea

Our simulations indicate that Rhea must have experienced elevated heat flows reaching at least a few tens of mW m^{-2} at some point in its history in order to account for the present basin relaxation fractions (Fig. 6). This finding is supported by those of Nimmo et al. (2010), who used limb profiles to investigate the long-wavelength topography and topographic variance spectrum of Rhea, and inferred a heat flux of 15 mW m^{-2}, although our simulations imply a heat flow even higher than this by several mW m^{-2}. The fact that only impact basins above a certain diameter (~100 km) appear to be relaxed, regardless of their location on Rhea, implies that such a heating event was global in its extent, with no localized relaxation of craters of all sizes such as that seen on Enceladus (Spencer et al., 2009). This is consistent with the assertion of Lissauer et al. (1988) that there is no statistically significant evidence for local endogenic resurfacing on Rhea based on analysis of the spatial distribution of craters, although their investigation was based on Voyager data and was not global in its extent. The duration of elevated heat flow is relatively unconstrained, as relaxation fractions are virtually identical for relaxation timescales of 10 Myr, 100 Myr, and 1 Gyr. Our simulations are currently limited to modeling constant heat flow; in reality, the progressively dropping heat flow following an elevation would reduce the differences between relaxation fractions that we observe for the different relaxation timescales that we model. However, given that there is little difference between the relaxation fractions even for the constant heat flows that we use (see Fig. 6), any reduction in the differences that is accomplished by modeling a decreasing heat flow would be negligible compared to what we already see.

There are various sources of heat for the mid-sized icy satellites, notably heat of accretion, radioactive isotopes, despinning, and tidal dissipation (Peale, 1977, 1999; Ellsworth and Schubert, 1983; Matson et al., 2009). The relative significance of these sources with respect to accounting for why Rhea experienced a global spike in heating, and Iapetus did not, will depend on their timing and the amount of heat they provide, which in turn depends on the model used for the satellites' formation. We consider a model recently introduced by Charnoz et al. (2011), following on numerical simulations of ring and satellite formation in the Saturnian system (Canup and Ward, 2006; Canup, 2010), to explain the formation of Saturn's mid-sized icy satellites interior to and including Rhea via accretion from the outer edge of a giant icy ring system that resulted from stripping of material from a Titan-sized body by tidal forces. As each satellite achieves a certain mass threshold, resonant torques would drive it from the ring, and the satellite's orbit would evolve outwards due to tidal interaction with Saturn, with a new satellite subsequently being spawned at the ring edge (Canup, 2010); Rhea would therefore be the first mid-sized icy satellite to spawn. Their simulations are consistent with moonlet accretion that has been observed at the edge of the present-day rings (corresponding to the Roche limit) by the Cassini orbiter (Charnoz et al., 2010).

Accretion: The model of Charnoz et al. (2011) postulated that small proto-satellites would accrete from the ring, with silicate cores and icy shells, and would eventually coalesce to create the fully formed satellites. The initial temperatures of the satellites are a function of the temperature of the accreting proto-satellites as well as accretional heat from their kinetic energy (Castillo-Rogez et al., 2007). In contrast to large icy satellites, accretional heating is not considered to be a significant heat source that could drive early melting and separation of silicates from a volatile phase in small satellites (Squyres et al., 1988; Matson et al., 2009; Charnoz et al., 2011). The temperature increase associated with accretion is thought to be similar for Rhea and Iapetus given their comparable sizes (Ellsworth and Schubert, 1983), with temperatures at the end of accretion estimated to be 160 K for Iapetus and 200 K for Rhea. The temperature of the newly formed Rhea would have been above the water ice creep temperature of ~170 K, which would potentially permit substantial deformation on a geologic time scale; however, accretion does not contribute significantly to warming the interior because most of its heat is deposited close to the surface (~20 km depth) where it is conducted upward and then radiated to space (Squyres et al., 1988).

Despinning: A significant difference between the evolutions of Iapetus and Rhea (indeed Iapetus and the rest of the mid-sized icy satellites) is that of their orbital dynamics, which is intimately linked to their thermal evolution. Rhea's relative proximity to Saturn would have resulted in a despinning time for Rhea of ~10^4 years (Castillo-Rogez et al., 2007). Heat provided by Rhea's despinning, which may entail a global temperature increase of up to 20 K integrated over the despinning time (Matson et al., 2009), would therefore have been provided over a very short interval relative to Iapetus, where any heating provided by despinning would have been protracted over several hundred million to billions of years (see section 6.1).

Tidal dissipation: Charnoz et al. (2011) noted that a consequence of their model is the likely occurrence of high eccentricity episodes early in the satellite's histories, generated by mutual perturbations and close encounters between the satellites, and suggested that these episodes would have had thermal consequences for the larger satellites such as Rhea. Enhanced tidal dissipation within Rhea's interior associated with these high orbital eccentricities would have been an important source of heat in its post-accretion phase. In contrast, the isolated position and stable orbit of Iapetus would prevent any such tidal interaction over the course of its history (Singer and McKinnon, 2010; Robuchon et al., 2011).

Radioactive isotopes and differentiation: The decay of short-lived radioactive isotopes (SLRIs) within the satellites would provide a strong heat pulse during the first 10 Myr following planet formation (if the satellites had formed by this time), while the decay of long-lived radioactive isotopes (LLRIs) would have provided a weaker, prolonged heat flux over the entire histories of the satellites (Matson et al., 2009). The proportion of radionuclides incorporated by the satellites during accretion will depend on their rock content. The current estimate for the mass ratio of rocky core to icy mantle in Iapetus is 20:80 (Castillo-Rogez et al. (2007) and Robuchon et al. (2010), based on calculation of its mean density), and for Rhea, estimates range from 36:64 (Thomas et al. (2007), based on measurement of its shape using limb coordinates and stereogrammetric control points) to 25:75 (Anderson and Schubert (2007; 2010), based on calculations of its mean density and axial moment of inertia). Based on these estimates, Rhea could therefore contain between a 25% to 80% higher abundance of radionuclides relative to Iapetus, assuming an equal proportion of radionuclides in the rock-forming material for both of them. The distribution of the silicate and ice components of the respective satellites would influence the rheology of the surficial ice in which the impact basins form: a high proportion of rock within the ice would provide a non-viscous component that would inhibit relaxation, but only to a minor degree given the low rock abundances within Rhea and Iapetus (Durham et al., 1997). In addition, differentiation of a satellite's interior into a rocky core and an icy mantle would result in conversion of gravitational potential energy into a further source of heat (Leliwa-Kopystynski and Kossacki, 2000). Robuchon et al. (2010) infer an undifferentiated interior for Iapetus throughout its evolution, based on calculations of its internal Rayleigh number, volumetric rock fraction and internal temperature, and Castillo-Rogez et al. (2007) treat Iapetus as being undifferentiated in their modeling. However, geophysical investigations of the interior of Rhea using Cassini data have proven somewhat inconclusive. Independent studies by Anderson and Schubert (2007) and Iess et al. (2007) inferred the interior to be an undifferentiated mixture of rock-metal and water ice, with a thin surface layer of pure water ice, based on measurements of its mass and quadrupole gravity moments from a single Cassini flyby in 2005. However, this interpretation has been questioned (Mackenzie et al., 2008), and despite a rebuttal to these concerns by Anderson and Schubert (2010), it is generally regarded that further gravity flybys of Rhea are required to refine the model of its internal structure (Nimmo et al., 2010). Theoretically, the formation scenario of the inner, mid-sized icy satellites developed by Charnoz et al. (2011) implies that these satellites were differentiated to a high degree after their accretion. In addition, the high global heat flow that we have derived from our basin relaxation simulations would likely have raised the interior to a temperature sufficient to cause the ice to undergo ductile creep at fairly shallow depths (tens of kilometers), which would facilitate the gravity-driven mechanical separation of ice and rocky material and leave the subsurface deficient in rocky material that would impede relaxation. Yet if Rhea were in fact to be undifferentiated, and in place of pure ice in the shallow subsurface there is instead a homogeneous rock-ice mixture at the rock-ice mass ratio of Rhea (i.e. ~30:70), then the corresponding increase in viscosity would be by a factor of 10 to 25 (Durham et al., 1997), which could be compensated for by an increase in heat flow of only 10 to 20%.

Castillo-Rogez et al. (2007) describe how early heating of Rhea would have resulted in a lithosphere too thin (<5 km) to support any significant non-hydrostatic loads. Any deep basins on Rhea would therefore have relaxed swiftly after their formation. If the large basins we see on Rhea formed synchronously with the heat pulse provided by tidal dissipation, rapid despinning, and decay of SLRIs, with the smaller, superimposing craters forming after the main era of relaxation, then this would require that the large basins form within the first few tens of Myr of Rhea's formation, meaning that they would be representative of the late phase of accretion.

6.3 Large basin frequencies on Iapetus and Rhea

The fact that Iapetus displays more large basins (20) than Rhea (13), despite being located further away from Saturn, where the impact flux is lower, is an apparent contradiction. Lissauer et al. (1988) suggested two possible explanations for the differing cratering records: either that the surface of Iapetus is older than that of Rhea, or that Iapetus was bombarded by a population of Saturn-orbiting debris that did not extend inward to Rhea. The model of Charnoz et al. (2011) would be consistent with the former explanation, as it requires the satellites' formation to be tied to the rings' formation, which may have occurred anytime between 2.5 and 4.5 Gyr ago. This would imply that Rhea may have accreted as little as 2.5 Gyr ago and would therefore not have accumulated large impacts from heliocentric impactors like Iapetus did, given that Iapetus formed contemporaneously with Saturn 4.5 Gyr ago. Charnoz et al. (2011) considered their model to support the hypothesis that Saturn's inner icy satellites, including Rhea, were hit by a population of planetocentric impactors that comprised the fragments of an intense post-accretional phase for those satellites completing their accretion beyond ~200,000 km from Saturn's center, although they do acknowledge the viability of an alternative scenario whereby planetesimals impact the mid-sized satellite just after accretion from Saturn's nebula (Mosqueira and Estrada, 2003). Based on our relaxation simulations, we propose that shortly after formation, Rhea would have accumulated a population of large impact basins (either from heliocentric or planetocentric impactors) that would have quickly relaxed due to the high heat flux that predominated during this era. In order for the topographic signatures of these lost basins to be erased, it is likely that they relaxed to the extent that they became (or nearly became) palimpsests, with their floors uplifting to the level of the surrounding terrain. Our simulations indicate that as little as several Myr of relaxation under high heat flow conditions is sufficient for these basins to relax to presently observed relaxation fractions, meaning that the formation time of Rhea (4.5 to 2.5 Gyr ago) cannot be constrained based on our simulations, although our crater counts (Table 5) would indicate formation contemporaneous with Saturn's. Any remaining relief, including the central peaks and rims of the basins (which would not have been significantly affected by the relaxation), would have to have been eroded by subsequent impacts and ejecta cover. We have identified only two large and very poorly preserved provisional impact basins on Rhea, which are virtually undetectable in the Cassini global mosaic of Rhea, but which exhibit a topographic signature in our global DEM. Their centers are located at 42.5°S, 176.5°W, and 15.5°S, 20.7°W (see Fig. 1), the former taking the form of an annular trough with a central rise, and the latter, a flat-floored circular depression. These features may represent examples of a first generation of large impacts, their morphologies having not been completely erased by relaxation and subsequent bombardment. The comparatively better-preserved basins on Rhea, including Tirawa, Mamaldi, Izanagi and Powehiwehi, would have formed when the phase of high heat flux and bombardment flux was diminishing, meaning that their morphologies did not relax to the same degree as their precursors, and were not eroded to the same degree by later impacts. In contrast, the relief of large basins that did accumulate on Iapetus has not been affected by relaxation, and those we do see have not been erased by later impacts. We have identified at least one highly degraded and very ancient basin on Iapetus (center location 44.3°N, 311.7°W, see Fig. 1), yet it is poorly observed and not well understood at present.

6.4 Comparison with the Galilean satellites

The rapid relaxation of basin morphologies on Rhea within the first tens to hundreds of millions of years after formation, and the subsequent reduced relaxation rate, mirrors the results of the relaxation simulations of Dombard and McKinnon (2006) for Callisto and Ganymede. As described by Dombard and McKinnon (2006), the phenomenon can be attributed to the viscoelastic rheology of the ice shells of the satellites, whereby viscosity decreases with depth, creating a high-viscosity surface layer (essentially a lithosphere) that is underlain by a low-viscosity interior, with ductile creep being a more efficient process in the latter compared to the former. The overlying lithosphere will flex in response to surface topography, and in the case of an impact basin will flex upwards quickly due to the negative mass load on the surface. A much slower evolution of the lithosphere then progresses, as creep in the lithosphere slowly relaxes stresses within itself, effectively thinning it and permitting more flexure as time passes. However, the efficiency of creep in the lithosphere is influenced by the surface temperature: a low surface temperature will limit creep and slow the later stage of deformation even further (Damptz and Dombard, 2011). Surface temperatures on Ganymede and Callisto are estimated to range between ~80 and ~130 K (e.g., Herrick and Stevenson, 1990); the surface temperature on Rhea is estimated to range between ~53 and ~99 K (Khurana et al., 2008). The later, slower stage of relaxation will therefore progress at an even slower rate on Rhea than it would on Ganymede or Callisto, meaning that total relaxation on Rhea is virtually the same for all relaxation timescales; for Ganymede or Callisto, there is a greater difference between relaxation fractions for different relaxation timescales (see Fig. 9 in Dombard and McKinnon, 2006).

7. Conclusions

We have generated DEMs of the surfaces of Rhea and Iapetus using Cassini data and used them to obtain crater d/D plots for both satellites and topographic profiles of large basins on each of them. Our plots show that craters of all sizes on Iapetus have experienced minimal relaxation, with the larger basins (D > 200 km) reaching depths greater than 10 km, while on Rhea relaxation only affects craters above ~100 km in diameter, with none reaching depths greater than ~6.5 km. The similar sizes of Rhea and Iapetus render the effects of gravitational acceleration negligible when comparing crater morphologies on the two satellites. Treating the profiles of the Iapetus basins as analogues for the profiles of the initial, unrelaxed Rhea basins, the d/D plots of both satellites have been used to gauge the magnitude of basin relaxation on Rhea. Most of the basins on Rhea display relaxation fractions that coincide with or exceed the standard fraction of 0.632.

In order to deduce the conditions that led to the differing relaxation states of basins on Rhea and Iapetus, relaxation simulations have been performed for two basin size classes in order to find the combination of relaxation timescale and heat flow that accounts for the present relaxation magnitude observed for each size class on each satellite. Our simulations indicate that Iapetus has experienced only radiogenic heat flow of no more than a few mW m^{-2} over the course of its history, while Rhea must have experienced a period of elevated heat flow reaching at least a few tens of mW m^{-2}; in all simulation cases, the majority of the total observed relaxation occurs within several hundred Myr after formation of the basin, meaning that heat flow is more influential than relaxation timescale in determining the final relaxation fraction of a basin. This result is consistent with analogous relaxation simulations performed for craters on Ganymede and Callisto by Dombard and McKinnon (2006).

We have considered potential heat sources as well as our own estimates of the ages of two basins on Rhea in order to identify the timing and cause of Rhea's increased heat flow that led to such relaxation. The model of Charnoz et al. (2011) for the formation of Saturn's mid-sized icy satellites interior to and including Rhea describes how Rhea's orbit would have expanded outwards after its accretion from a giant primordial ring. This post-accretional phase would have been associated with heating of Rhea deriving from rapid despinning (Castillo-Rogez et al., 2007; Matson et al., 2009) as well as strong tidal interactions with Saturn and other satellites caused by changing orbital eccentricities and resonances (Canup and Ward, 2006; Canup, 2010; Charnoz et al., 2011). In contrast, Iapetus' isolated position at the periphery of the system has ensured that it has remained dynamically inert over its entire history, and has experienced negligible heating originating from despinning and tidal dissipation (Castillo-Rogez et al., 2007). Additionally, based on estimates of the ratios of rocky core to icy mantle in Iapetus and Rhea, it is likely that Rhea had a modestly higher concentration of SLRIs than Iapetus after formation, the rapid decay of which would have heated Rhea's interior to a greater extent than Iapetus'. If responsible, these various heating mechanisms (SLRIs, despinning and tidal dissipation) would have provided an elevated heat flow early in Rhea's history, likely within the first ~10 Myr after its formation, thereby placing a constraint on the timing of formation of its large basins, which would have both formed and relaxed by the end of this early heat pulse. If so, then basin crater statistics could provide a key anchor for the time-stratigraphy and chronology of these satellites.

Pending updates to bombardment flux estimates, we have derived crater age estimates for Powehiwehi and Tirawa based on the Zahnle et al. (2003) and Neukum et al. (2006) functions. Our Zahnle-based basin ages extend to 4.5 Gyr, while the Neukum ages extend to 4.36 Gyr, although with considerable uncertainty. Overlap of basin formation with the early heat pulse is therefore plausible, although our age range does extend to times later than its occurrence. The results of the modeling of

Charnoz et al. (2011) are consistent with Rhea accreting from the primordial ring at any time between 4.5 and 2.5 Gyr ago, but our small crater counts indicate a formation contemporaneous with that of Saturn. We do not currently know of a heating mechanism able to provide tens of mW m^{-2} to the thermal output of Rhea that would occur later than this early heating phase, with the exception of speculative later resonance periods. We have identified provisional and highly degraded large basins on Rhea that may be representatives of a 'first generation' of basins that were mostly eliminated by a combination of relaxation and bombardment prior to the formation of the better-preserved large basins.

Acknowledgements

This study was supported by the NASA Cassini Data Analysis Program and the LPI Postdoctoral Fellows fund. We would like to acknowledge the input of Dr. Michelle Kirchoff of the Southwest Research Institute, Boulder, who aided us in our derivation of crater ages for two basins on Rhea using the Zahnle et al. (2003) function. Two anonymous reviews were beneficial to enhancing manuscript clarity.

References

Anderson, J.D., Schubert, G., 2007. Saturn's satellite Rhea is a homogeneous mix of rock and ice. Geophys. Res. Lett. 34, L02202, doi:10.1029/2006GL028100.

Anderson, J.D., Schubert, G., 2010. Rhea's gravitational field and interior structure inferred from archival data files of the 2005 Cassini flyby. Phys. Earth Planet. Int. 178, 176-182.

Barr, A.C., McKinnon, W.B., 2006. Convection in Titan, Ganymede, and Callisto with Self-Consistent Ice Grain Size. Bull. Am. Astron. Soc. 38, 587.

Bland, M.T., Singer, K.N., McKinnon, W.B., Schenk, P.M., 2012. Crater relaxation on Enceladus: Tales of high heat fluxes in unexpected places. Lunar Planet. Sci. XLIII, abstract #2168.

Bonner, W.J., Schmall, R.A., 1973. A photometric technique for determining planetary slopes from orbital photographs. U.S. Geol. Surv. Prof. Pap., 812-A.

Canup, R.M., 2010. Origin of Saturn's rings and inner moons by mass removal from a lost Titan-sized satellite. Nature 468, 943-946.

Canup, R.M., Ward, W.R., 2006. A common mass scaling for satellite systems of gaseous planets. Nature 441, 834-839.

Castillo-Rogez, J.C., Matson, D.L., Sotin, C., Johnson, T.V., Lunine, J.I., Thomas, P.C., 2007. Iapetus' geophysics: Rotation rate, shape and equatorial ridge. Icarus 190, 179-202.

Castillo-Rogez, J.C., Efroimsky, M., Lainey, V., 2011. The tidal history of Iapetus: Spin dynamics in the light of a refined dissipation model. J. Geophys. Res. 116, E09008, doi:10.1029/2010JE003664.

Charnoz, S., Salmon, J., Crida, A., 2010. The recent formation of Saturn's moonlets from viscous spreading of the main rings. Nature 465, 752-754.

Charnoz, S., et al., 2011. Accretion of Saturn's mid-sized moons during the viscous spreading of young massive rings: Solving the paradox of silicate-poor rings versus silicate-rich moons. Icarus 216, 535-550.

Cruikshank, D.P., et al., 2005. A spectroscopic study of the surfaces of Saturn's large satellites: H_2O ice, tholins, and minor constituents. Icarus 175, 268-283.

Damptz, A.L., Dombard, A.J., 2011. Time-dependent flexure of the lithospheres on the icy satellites of Jupiter and Saturn. Icarus 216, 86-88.

Dombard, A.J., 2000. Modeling of geodynamic processes on Ganymede and Callisto: Insight into thermal and tectonic histories. Dissertation Abstracts International, 61-09, Section B, page 4625.

Dombard, A.J., McKinnon, W.B., 2000. Long-term retention of impact crater topography on Ganymede. Geophys. Res. Lett. 27, 3663-3666.

Dombard, A.J., Gillis, J.J., 2001. Testing the viability of topographic relaxation as a mechanism for the formation of lunar floor-fractured craters. J. Geophys. Res. 106, 27,901-27,909.

Dombard, A.J., McKinnon, W.B., 2006. Elastoviscoplastic relaxation of impact crater topography with application to Ganymede and Callisto. J. Geophys. Res. 111, E01001, doi:10.1029/2005JE002445.

Dombard, A.J., Bray, V.J., Collins, G.S., Schenk, P.M., Turtle, E.P., 2007. Relaxation and the Formation of Prominent Central Peaks in Large Craters on the Icy Satellites of Saturn. Bull. Am. Astron. Soc. 39, 429.

Dombard, A.J., Schenk, P.M., Turtle, E.P., Lederer, A.P., 2009. Relaxation of "Fresh" Large Craters on the Icy Galilean Satellites and the Depths to Their Oceans. American Geophysical Union, Fall Meeting 2009, abstract #P51E-1170.

Dougherty, M.K., Esposito, L.W., Krimigis, S.M., 2009. Overview. In: Dougherty, M., Esposito, L., Krimigis, S. (Eds.), Saturn from Cassini-Huygens, Springer NY, pp. 1-8.

Durham, W.B., Kirby, S.H., Stern, L.A., 1997. Creep of water ices at planetary conditions: A compilation. J. Geophys. Res. 102, 16,293-16,302.

Ellsworth, K., Schubert, G., 1983. Saturn's icy satellites – Thermal and structural models. Icarus 54, 490-510.

Gammon, P.H., Kiefte, H., Clouter, M.J., 1983. Elastic constants of ice samples by Brillouin spectroscopy. J. Phys. Chem. 87, 4025–4029.

Gehrels, T., Matthews, M.S. (Eds.), 1984. Saturn, Univ. Ariz. Press, Tucson, 968 pp.

Giese, B., et al., 2008. The topography of Iapetus' leading side. Icarus 193, 359-371.

Goldsby, D.L., Kohlstedt, D.L., 2001. Superplastic deformation of ice: Experimental observations. J. Geophys. Res. 106, 11,017-11,030.

Hartmann, W.K., 1972. Interplanet variations in the scale of crater morphology – Earth, Mars, Moon. Icarus 17, 707-713.

Herrick, D.L., Stevenson, D.J., 1990. Extensional and compressional instabilities in icy satellite lithospheres. Icarus 85, 191-204.

Iess, L., Rappaport, N.J., Tortora, P., Lunine, J., Armstrong, J.W., Asmar, S.W., Somenzi, L., Zingoni, F., 2007. Gravity field and interior of Rhea from Cassini data analysis. Icarus 190, 585-593.

Jaumann, R., et al., 2009. Icy Satellites: Geological Evolution and Surface Processes. In: Dougherty, M., Esposito, L., Krimigis, S. (Eds.), Saturn from Cassini-Huygens, Springer NY, pp. 637-681.

Khurana, K.K., Russell, C.T., Dougherty, M.K., 2008. Magnetic portraits of Tethys and Rhea. Icarus 193, 465-474.

Klinger, J., 1980. Influence of a phase transition of ice on the heat and mass balance of comets. Science 209, 271– 272.

Leliwa-Kopystynski, J., Kossacki, K.J., 2000. Evolution of porosity in small icy bodies. Planet. Space Sci. 48, 727–745.

Lissauer, J.J., Squyres, S.W., Hartmann, W.K., 1988. Bombardment History of the Saturn System. J. Geophys. Res. 93, 13,776-13,804.

Mackenzie, R.A., Iess, L., Tortora, P., Rappaport, N.J., 2008. A non-hydrostatic Rhea. Geophys. Res. Lett. 35, L05204, doi:10.1029/2007GL032898.

Matson, D.L., Castillo-Rogez, J.C., Schubert, G., Sotin, C., McKinnon, W.B., 2009. The Thermal Evolution and Internal Structure of Saturn's Mid-Sized Icy Satellites. In: Dougherty, M., Esposito, L., Krimigis, S. (Eds.), Saturn from Cassini-Huygens, Springer NY, pp. 577-612.

McKinnon, W.B., 1999. Convective instability in Europa's floating ice shell. Geophys. Res. Lett. 26, 951-954.

McKinnon, W.B., 2002. On the initial thermal evolution of Kuiper Belt objects. In: Proceedings of Asteroids, Comets, Meteors - ACM 2002, 29-38, ed. Warmbein, B., publ. ESA Publications Division, Noordwijk, Netherlands.

Melosh, H.J., 1977. Crater modification by gravity: A mechanical analysis of slumping. In: Roddy, D.J., Pepin, R.O., Merrill, R.B. (Eds.), Impact and Explosion Cratering, Pergamon NY, pp. 1245-1260.

Moore, J.M., Schenk, P.M., 2007. Topography of endogenic features on Saturnian mid-sized satellites. Lunar Planet. Sci. XXXVIII, abstract #2136.

Moore, J.M., Schenk, P.M., Bruesch, L.S., Asphaug, E., McKinnon, W.B., 2004. Large impact features on middle-sized icy satellites. Icarus 171, 421-443.

Morrison, D., Owen, T., Soderblom, L.A., 1986. The satellites of Saturn. In: Burns, J.A., Matthews, M.S. (Eds.), Satellites, Univ. Ariz. Press, Tucson, pp. 764-801.

Mosqueira, I., Estrada, P.R., 2003. Formation of the regular satellites of giant planets in an extended gaseous nebula. II: Satellite migration and survival. Icarus 163, 232–255.

Neukum, G., Wagner, R., Wolf, U., Denk, T., 2006. The cratering record and cratering chronologies of the saturnian satellites and the origin of impactors: Results from Cassini ISS data. European Planetary Science Congress, Berlin, Germany, p.610.

Nimmo, F., Bills, B.G., Thomas, P.C., Asmar, S.W., 2010a. Geophysical implications of the long-wavelength topography of Rhea. J. Geophys. Res. 115, E10008, doi:10.1029/2010JE003604.

Orton, G.S., et al., 2009. Review of Knowledge Prior to the Cassini-Huygens Mission and Concurrent Research. In: Dougherty, M., Esposito, L., Krimigis, S. (Eds.), Saturn from Cassini-Huygens, Springer NY, pp. 9-54.

Passey, Q.R., 1982. Viscosity structure of the lithospheres of Ganymede, Callisto and Enceladus, and of the Earth's mantle. Thesis, Calif. Inst. of Technol., Pasadena.

Passey, Q.R., 1983. Viscosity of the lithosphere of Enceladus. Icarus 53, 105-120.

Passey, Q.R., Shoemaker, E.M., 1982. Craters and basins on Ganymede and Callisto - Morphological indicators of crustal evolution. In: Morrison, D., Matthews, M.S. (Eds.), Satellites of Jupiter, Univ. of Ariz. Press, Tucson, pp. 379–434.

Peale, S.J., 1977. Rotational histories of the natural satellites. In: Burns, J.A. (Ed.), Planetary Satellites, Univ. of Ariz. Press, Tucson, pp. 87–112.

Peale, S.J., 1999. Origin and evolution of the natural satellites. Annu. Rev. Astron. Astrophys. 37, 533-602.

Phillips, C.B., Hammond, N.P., Robuchon, G., Nimmo, F., Beyer, R., Roberts, J., 2012. Stereo imaging, crater relaxation, and thermal histories of Rhea and Dione. Lunar Planet. Sci. XLIII, abstract #2571.

Pike, R.J., 1974. Depth/diameter relations of fresh lunar craters: revision from spacecraft data. Geophys. Res Lett. 1, 291-294.

Pike, R.J., 1980. Control of crater morphology by gravity and target type: Mars, Earth, Moon. Lunar Planet. Sci. XI, 2159-2189.

Quaide, W. L., Gault, D. E., Schmidt, R. A., 1965. Gravitative effects on lunar impact structures. Ann. N.Y. Acad. Sci. 123, 563–572.

Robuchon, G., Choblet, G., Tobie, G., Cadek, O., Sotin, C., Grasset, O., 2010. Coupling of thermal evolution and despinning of early Iapetus. Icarus 207, 959–971.

Robuchon, G., Nimmo, F., Roberts, J., Kirchoff, M., 2011. Impact basin relaxation at Iapetus. Icarus 214, 82-90.

Schenk, P.M., 1989. Crater Formation and Modification on the Icy Satellites of Uranus and Saturn: Depth/Diameter and Central Peak Occurrence. J. Geophys. Res. 94, 3813-3832.

Schenk, P.M., 2002. Thickness constraints on the icy shells of the Galilean satellites from a comparison of crater shapes. Nature 417, 419-421.

Schenk, P.M., Bulmer, M.H., 1998. Origin of Mountains on Io by Thrust Faulting and Large-Scale Mass Movements. Science 279, 1514-1517.

Schenk, P.M., Williams, D.A., 2004. A potential thermal erosion lava channel on Io. Geophys. Res. Lett. 31, doi:10.1029/2004GL021378.

Schenk, P.M., McEwen, A., Davies, A.G., Davenport, T., Jones, K., 1997. Geology and topography of Ra Patera, Io, in the Voyager era: prelude to eruption. Geophys. Res. Lett. 24, 2467-2470.

Schenk, P.M., Wilson, R.R., Davies, A.G., 2004. Shield volcano topography and the rheology of lava flows on Io. Icarus 169, 98-110.

Schubert, G., Spohn, T., Reynolds, R.T., 1986. Thermal histories, compositions and internal structures of the moons of the Solar System. In: Burns, J.A., Matthews, M.S. (Eds.), Satellites, Univ. Ariz. Press, Tucson, pp. 224-292.

Seal, D., Buffington, B., 2009. The Cassini Extended Mission. In: Dougherty, M., Esposito, L., Krimigis, S. (Eds.), Saturn from Cassini-Huygens, Springer NY, pp. 725-744.

Singer, K., McKinnon, W.B., 2010. Iapetian tectonics: Despinning, respinning, contraction, or something completely different? In: DPS meeting, tome 42 of Bulletin of the American Astronomical Society, p. 941.

Smith, B.A., et al., 1981. Encounter with Saturn: Voyager 1 imaging Science results. Science 212, 163-191.

Smith, B.A., et al., 1982. A new look at the Saturn system: The Voyager 2 images. Science 215, 505-537.

Spencer, J.R., et al., 2009. Enceladus: An Active Cryovolcanic Satellite. In: Dougherty, M., Esposito, L., Krimigis, S. (Eds.), Saturn from Cassini-Huygens, Springer NY, pp. 683-724.

Squyres, S.W., Reynolds, R.T., Summers, A.L., Shung, F., 1988. Accretional heating of the satellites of Saturn and Uranus. J. Geophys. Res. 93, 8779-8794.

Thomas, P.J., Squyres, S.W., 1988. Relaxation of Impact Basins on Icy Satellites. J. Geophys. Res. 93, 14,919-14,932.

Thomas, P.J., et al., 2007. Shapes of the saturnian icy satellites and their significance. Icarus 190, 573-584.

Turcotte, D.L., Schubert, G., 2002. Geodynamics: Applications of Continuum Physics to Geological Problems, John Wiley, Hoboken, NJ, 450 pp.

Turcotte, D.L., Willemann, R.J., Haxby, W.F., Norberry, J., 1981. Role of membrane stresses in the support of planetary topography. J. Geophys. Res. 86, 3951-3959.

Waite, J.H., et al., 2006. Cassini Ion and Neutral Mass Spectrometer: Enceladus Plume Composition and Structure. Science 311, 1419-1422.

Ward, W.R., 1981. Orbital inclination of Iapetus and the rotation of the Laplacian plane. Icarus 46, 97-107.

White, O.L., Schenk, P.M., 2011. Crater Shapes on the Saturnian Satellites: New Measurements Using Cassini Stereo Images. Lunar Planet. Sci. XLII, abstract #2136.

Williams, K.K., Zuber, M. T., 1998. Measurement and Analysis of Lunar Basin Depths from Clementine Altimetry. Icarus 131, 107-122.

Zahnle, K., Schenk, P., Levison, H., Dones, L., 2003. Cratering rates in the outer Solar System. Icarus 163, 263-289.

Figure captions

Figure 1. Global stereo-derived DEMs of Iapetus (a) and Rhea (b) in simple cylindrical projection, centered at 0°N, 180°W. The Iapetus DEM is at a resolution of 1 km/px, the Rhea DEM at 1.5 km/px. The vertical scales of both DEMs are stretched from +8 km to -8 km to highlight the contrast in vertical relief that the two satellites exhibit. The four letters are adjacent to the four largest named impact basins on Rhea: T = Tirawa, M = Mamaldi, P = Powehiwehi, I = Izanagi. The 'x's are placed in the centers of provisional, highly degraded, ancient impact basins that have been identified, one on Iapetus and two on Rhea.

Figure 2. Depth diameter measurements of simple and complex craters and large impact basins on Rhea and Iapetus with associated trendlines. The lunar (from Pike, 1980 and Williams and Zuber, 1998) and Ganymede (from Schenk, 2002) trends are plotted for comparison.

Figure 3. Averaged, symmetrical profiles of four large impact basins on Rhea and Iapetus. (a) Powehiwehi on Rhea and Naimon on Iapetus, each stretched to a diameter of 269 km. (b) Tirawa on Rhea and Falsaron on Iapetus, each stretched to a diameter of 419 km. For each pair, the profile of one basin has been shifted such that the level of its surrounding terrain matches that of the other.

Figure 4. Cassini imagery of four large craters of two size classes on Rhea and Iapetus, the morphologies of which are being used in our relaxation simulations. (a) Powehiwehi on Rhea, and (b) Naimon on Iapetus, representing the smaller size class, and (c) Tirawa on Rhea, and (d) Falsaron on Iapetus, representing the larger size class. All scale bars measure 100 km.

Figure 5. Radial topographic profiles resulting from viscoelastic simulations of basin relaxation on Rhea, assuming the isothermal, non-Newtonian rheology of ice. Lettered figures are grouped according to combinations of heat flow and ice grain size, with the timescale of relaxation being varied for each. (a-c)

show Powehiwehi/Naimon simulations, (d-f) show Tirawa/Falsaron simulations. For reference, measured profiles of unrelaxed Iapetus basins (in thick black) and relaxed Rhea basins (in thick gray) are included.

Figure 6. Relaxation fractions shown as a function of time for each of the simulation results shown in Fig. 5, represented as data points joined by logarithmic trendlines. Thick horizontal black and gray lines show the current *RF* values for Tirawa and Powehiwehi respectively. Vertical dashed line shows the age of the Solar System.

1. Coordinates and resolutions of Rhea and Iapetus DEMs that were used to make crater measurements.

te	Latitude limits of DEM (°N)	Longitude limits of DEM (°W)	DEM Resolution (km/px)	No. of craters measured in DEM	DEM type
	-90 to 90	0 to 360	1.5	12	Stereo
a	-43 to 7.8	158 to 173	0.14	62	Merged stereo/PC
	12 to 59	155 to 190	0.19	30	Merged stereo/PC
	-90 to 90	0 to 360	1	14	Stereo
	-18 to 23	120 to 170	0.35	6	Stereo
	-66 to -22	160 to 210	0.5	12	Stereo
	-47.3 to -40.5	205.5 to 212.2	0.15	3	Stereo
us	-65 to -27	190 to 227	0.43	8	Stereo
	-25 to 25	165 to 225	0.45	9	Stereo
	-40 to 30	270 to 305	0.45	3	Stereo
	-4.51 to 5.27	159.01 to 168.35	0.1	29	Stereo

Table 2. Least squares statistics of d/D plots for Rhea, Iapetus, and the Moon. Lunar values from *Pike (1980) and †Williams and Zuber (1998); Ganymede values from ‡Schenk (2002). Equation of the form $\log_{10}$ (depth) = $\log_{10}$ (depth at 1 km) + slope × $\log_{10}$ (diameter). *n* is the number of craters in the data sample. Values in parentheses are 95% (2σ) confidence limits.

Satellite	**Crater type**	***n***	**Slope**	**Depth at 1 km diameter**	**Mean d/D**
Rhea	Simple	63	0.808 (± 0.045)	0.289 (± 0.030)	0.221 (± 0.081)
	Complex	37	0.478 (± 0.028)	0.482 (± 0.042)	-
	Large basins	5	0.039 (± 0.353)	3.690 (± 0.900)	-
Iapetus	Simple	28	1.047 (± 0.053)	0.176 (± 0.028)	0.187 (± 0.047)
	Complex/Large basins	57	0.552 (± 0.026)	0.378 (± 0.043)	-
Moon	*Simple	179	1.013 (± 0.008)	0.195 (± 0.028)	0.199 (± 0.002)
	*Complex	47	0.313 (± 0.020)	1.088 (± 0.088)	-
	†Large basins	7	0.149	2.056	-
Ganymede	‡Simple	35	0.930 (± 0.042)	0.211 (± 0.011)	0.212 (± 0.064)
	‡Complex	40	0.422 (± 0.030)	0.293 (± 0.031)	0.097 (± 0.098)
	‡Central pit and central dome	15	-0.026 (± 0.135)	1.234 (± 0.237)	0.022 (± 0.017)

Table 3. Relaxation fractions of Rhea impact basins, measured relative to the Iapetus d/D trend. Values in parentheses are 95% (2σ) confidence limits.

Crater	***d*(*t*) (km)**	***d*(0) (km)**	**Δ*d* (km)**	***RF***
Izanagi	3.6 (± 0.73)	6.4 (± 0.22)	2.8 (± 0.95)	0.44 (± 0.16)
Powehiwehi	2.5 (± 0.35)	7.3 (± 0.26)	4.8 (± 0.61)	0.66 (± 0.11)
Tirawa	3.6 (± 1.08)	8.6 (± 0.42)	5.0 (± 1.50)	0.58 (± 0.20)
Mamaldi	3.1 (± 1.15)	9.5 (± 0.48)	6.4 (± 1.63)	0.67 (± 0.20)

Table 4. Diameter and depth statistics measured for four impact basins on Rhea and Iapetus. Diameter is measured from rim to rim and depth is measured from rim to floor. Values in parentheses are 95% (2σ) confidence limits.

Crater (Satellite)	**Diameter (km)**	**Depth (km)**	**Depth/Diameter**
Tirawa (Rhea)	397 (± 44.8)	5.6 (± 1.68)	0.014 (± 0.006)
Powehiwehi (Rhea)	268 (± 13.6)	3.7 (± 0.52)	0.014 (± 0.002)
Falsaron (Iapetus)	422 (± 22.0)	10.5 (± 4.44)	0.025 (± 0.012)
Naimon (Iapetus)	261 (± 31.0)	10.4 (± 1.24)	0.040 (± 0.010)

Table 5. Computed ages and age ranges of Powehiwehi and Tirawa impact basins as calculated using the case A scenario from Zahnle et al. (2003) and Neukum et al. (2006).

Basin	Zahnle age range	Zahnle age	Neukum age range	Neukum age
Powehiwehi	4.3 – 4.5 Ga	4.5 Ga	4.06 – 4.36 Ga	4.13 Ga
Tirawa	4.3 – 4.5 Ga	4.5 Ga	4.13 – 4.35 Ga	4.19 Ga

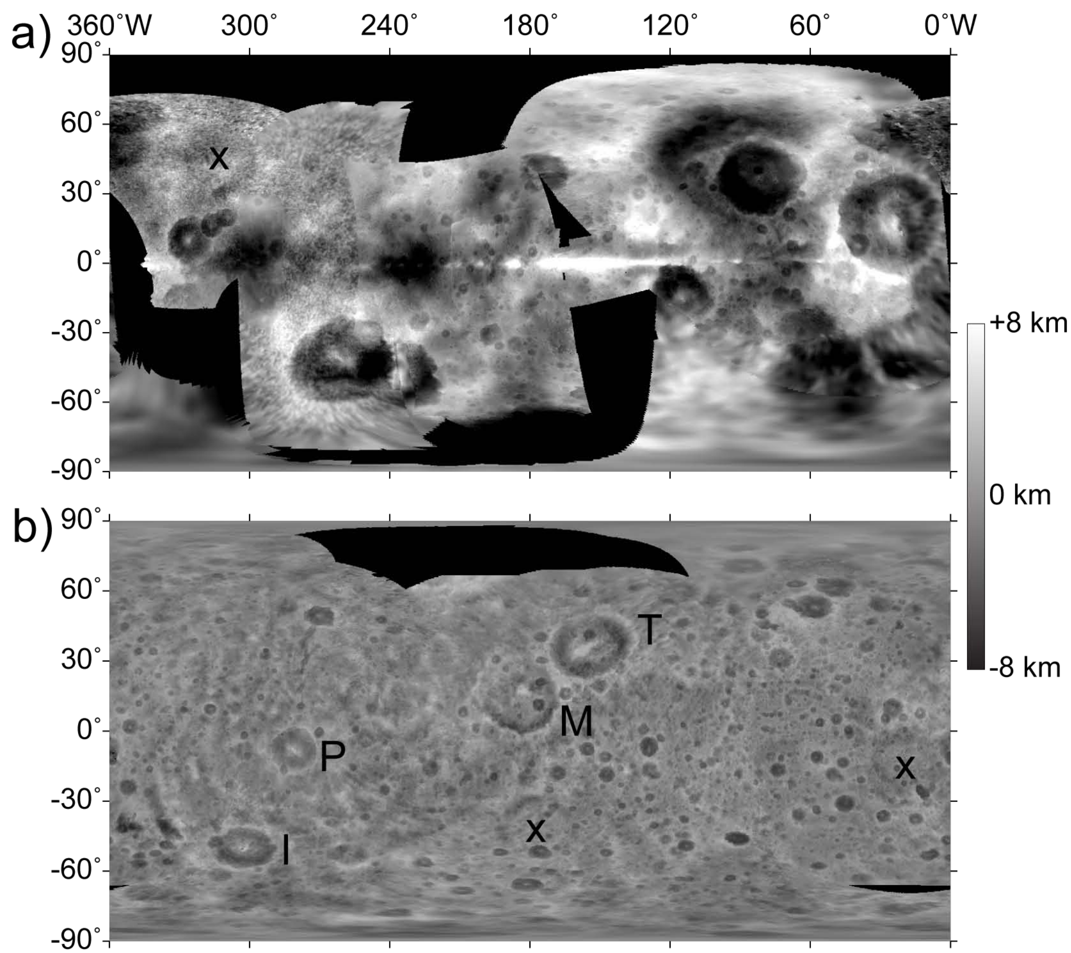

a)
360˚W
300˚
240˚
180˚
120˚
60˚
0˚W
90˚
60˚
30˚
0˚
-30˚
-60˚
-90˚
x
+8 km
0 km
-8 km
b)
T
M
P
I
x
x

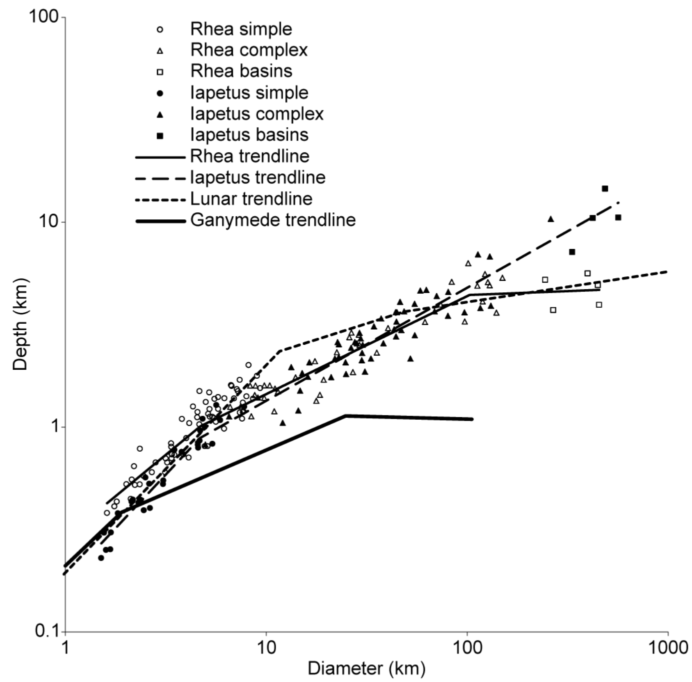

100
10
1
0.1
Depth (km)
1
10
100
1000
Diameter (km)
Rhea simple
Rhea complex
Rhea basins
Iapetus simple
Iapetus complex
Iapetus basins
Rhea trendline
Iapetus trendline
Lunar trendline
Ganymede trendline

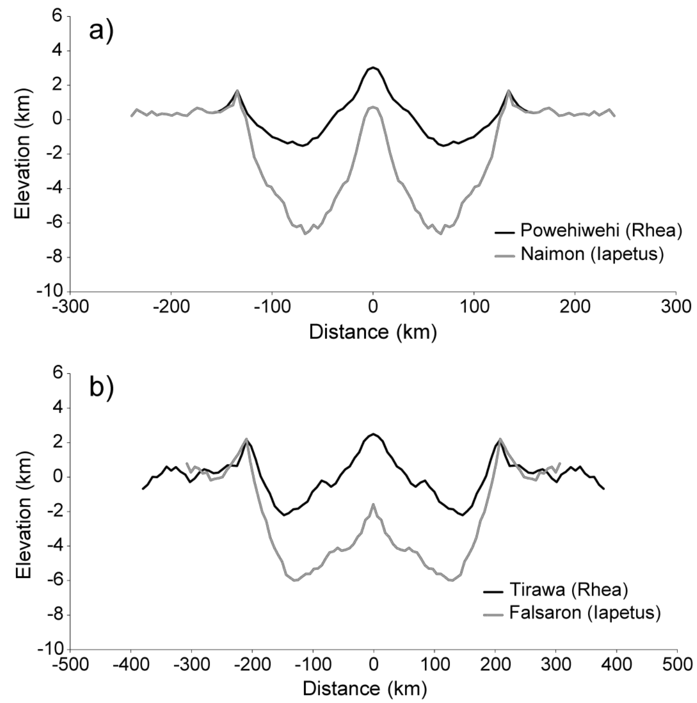
a)
Elevation (km)
Distance (km)
Powehiwehi (Rhea)
Naimon (Iapetus)
b)
Elevation (km)
Distance (km)
Tirawa (Rhea)
Falsaron (Iapetus)

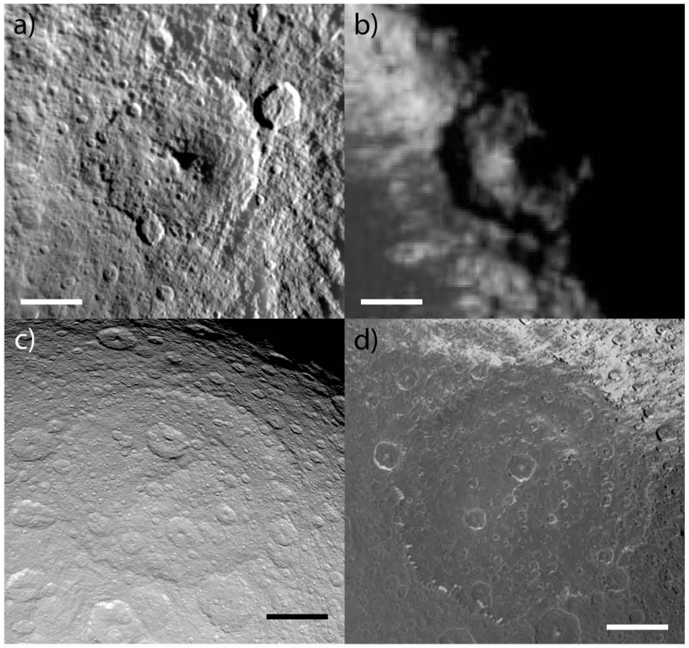
a)
b)
c)
d)

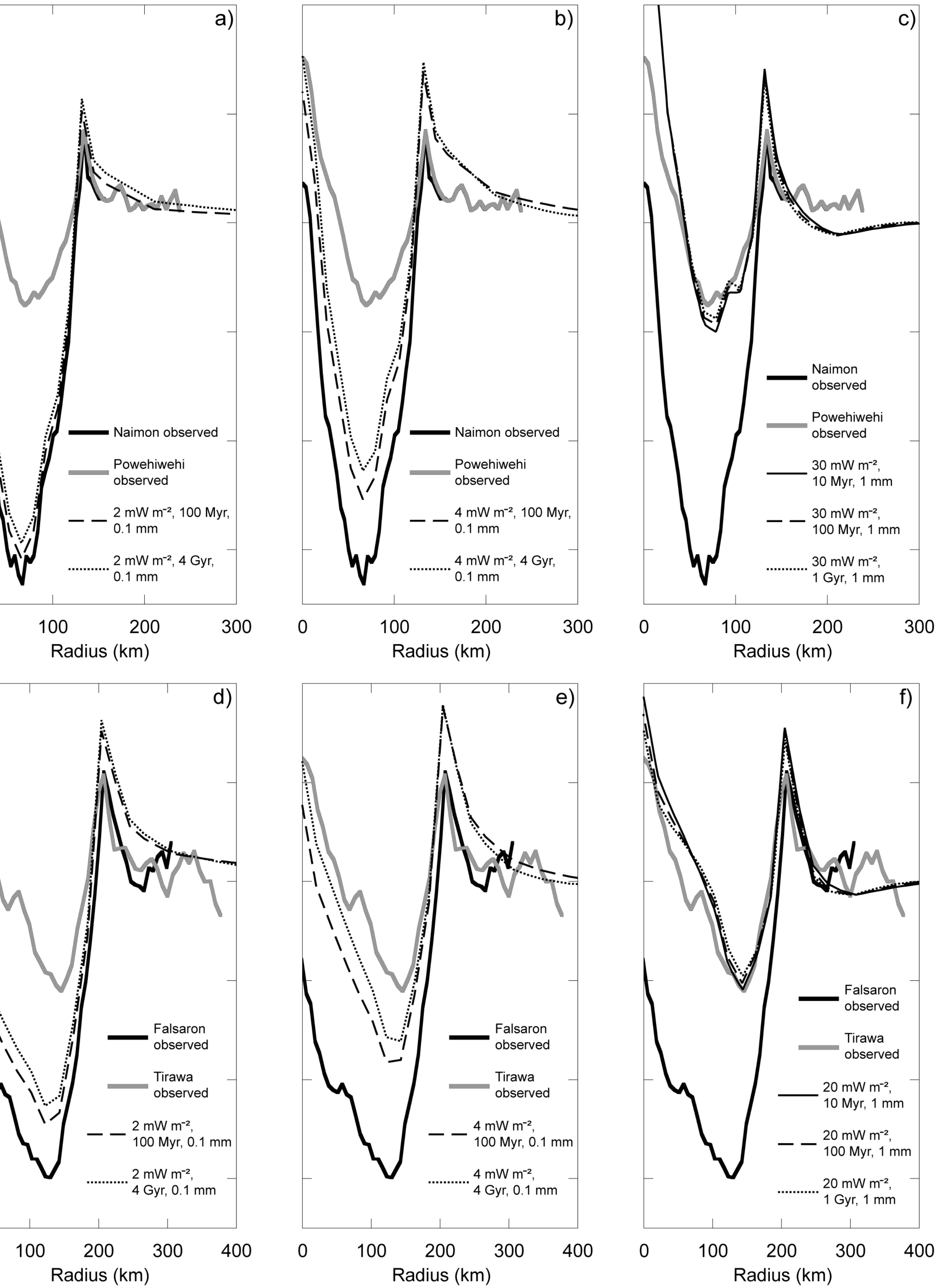
a)
Naimon observed
Powehiwehi observed
2 mW m⁻², 100 Myr, 0.1 mm
2 mW m⁻², 4 Gyr, 0.1 mm
100
200
300
Radius (km)
b)
Naimon observed
Powehiwehi observed
4 mW m⁻², 100 Myr, 0.1 mm
4 mW m⁻², 4 Gyr, 0.1 mm
0
100
200
300
Radius (km)
c)
Naimon observed
Powehiwehi observed
30 mW m⁻², 10 Myr, 1 mm
30 mW m⁻², 100 Myr, 1 mm
30 mW m⁻², 1 Gyr, 1 mm
0
100
200
300
Radius (km)
d)
Falsaron observed
Tirawa observed
2 mW m⁻², 100 Myr, 0.1 mm
2 mW m⁻², 4 Gyr, 0.1 mm
100
200
300
400
Radius (km)
e)
Falsaron observed
Tirawa observed
4 mW m⁻², 100 Myr, 0.1 mm
4 mW m⁻², 4 Gyr, 0.1 mm
0
100
200
300
400
Radius (km)
f)
Falsaron observed
Tirawa observed
20 mW m⁻², 10 Myr, 1 mm
20 mW m⁻², 100 Myr, 1 mm
20 mW m⁻², 1 Gyr, 1 mm
0
100
200
300
400
Radius (km)

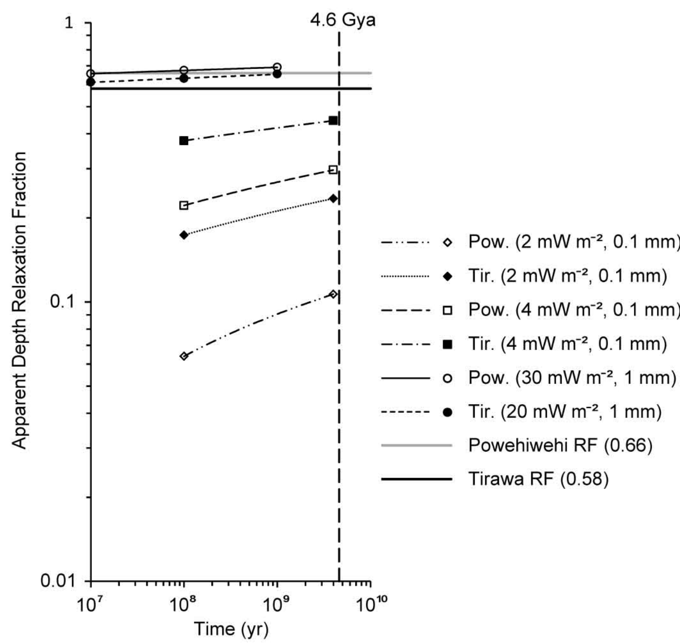

4.6 Gya
1
0.1
0.01
Apparent Depth Relaxation Fraction
10^7
10^8
10^9
10^10
Time (yr)
Pow. (2 mW m⁻², 0.1 mm)
Tir. (2 mW m⁻², 0.1 mm)
Pow. (4 mW m⁻², 0.1 mm)
Tir. (4 mW m⁻², 0.1 mm)
Pow. (30 mW m⁻², 1 mm)
Tir. (20 mW m⁻², 1 mm)
Powehiwehi RF (0.66)
Tirawa RF (0.58)